Biomaterials Science

PAPER

View Article Online
View Journal



Cite this: DOI: 10.1039/c8bm01188e

# Macromolecular crowding tunes 3D collagen architecture and cell morphogenesis†

S. K. Ranamukhaarachchi,‡ R. N. Modi,‡ A. Han, D. O. Velez, A. Kumar, A. J. Engler and S. I. Fraley *

Received 25th September 2018,
Accepted 21st November 2018

DOI: 10.1039/c8bm01188e

rsc.li/biomaterials-science

Collagen I is the primary extracellular matrix component of most solid tumors and influences metastatic progression. Collagen matrix engineering techniques are useful for understanding how this complex biomaterial regulates cancer cell behavior and for improving *in vitro* cancer models. Here, we establish an approach to tune collagen fibril architecture using PEG as an inert molecular crowding agent during gelation and cell embedding. We find that crowding produces matrices with tighter fibril networks that are less susceptible to proteinase mediated degradation, but does not significantly alter matrix stiffness. The resulting matrices have the effect of preventing cell spreading, confining cells, and reducing cell contractility. Matrix degradability and fibril length are identified as strong predictors of cell confinement. Further, the degree of confinement predicts whether breast cancer cells will ultimately undergo individual or collective behaviors. Highly confined breast cancer cells undergo morphogenesis to form either invasive networks reminiscent of aggressive tumors or gland and lobule structures reminiscent of normal breast epithelia. This morphological transition is accompanied by expression of cell–cell adhesion genes, including PECAM1 and ICAM1. Our study suggests that cell confinement, mediated by matrix architecture, is a design feature that tunes the transcriptional and morphogenic state of breast cancer cells.

## Introduction

Collagen is the most abundant matrix component within the tumor microenvironment,[1] and both clinical and *in vivo* studies have established the relevance of this particular ECM molecule in tumor progression. Collagen is both an independent clinical prognostic indicator of cancer progression[2] and a driver of tumorigenesis and metastasis.[3] As such, understanding how 3D collagen regulates cancer cell behavior could provide useful insights into disease pathogenesis and potential ECM targeted therapies.

The fibril architecture of collagen matrices has been implicated as a critical regulator of cancer cell behavior.[4–6] However, it remains challenging to systematically vary architectural features like pore size and fiber alignment without also changing matrix density or stiffness, which are known to modulate cell behavior in their own right.[7–9] Gelation temperature, pH, or density of collagen can be used to tune matrix architecture, but each of these approaches also alters matrix stiffness.[10–12] Magnetic, mechanical, and cell force driven reorganization of collagen fibrils as well as electrospinning can also be used to tune matrix architecture.[13–16] However, the resulting matrices present stiffness anisotropy to cells.[17–21] Collagen engineering techniques capable of modulating fibril characteristics independently of density and stiffness while also allowing cells to be fully embedded in 3D could lend new insight into how matrix architecture modulates cell behaviors.

Macromolecular crowding (MMC) is one possible approach to modulate fiber architecture without changing matrix stiffness or density. MMC is a phenomenon where high concentrations of macromolecules occupy space and generate excluded volume effects.[22,23] Various MMC agents have been used to effectively tune matrix properties for tissue engineering applications, including to promote cell-derived matrix deposition, to produce hierarchical porous structures in bioprinting applications, and to tune the reconstituted structure of tissue-derived matrices.[22,24–28] However, previous studies have tuned matrix stiffness simultaneously with fibril architecture.[24,25] Here, we sought to build on MMC-based matrix modification techniques to tune collagen matrix architecture (1) without changing matrix stiffness and (2) without direct effects of MMC on cell morphology migration or viability in fully embedded 3D culture.

*Bioengineering, University of California San Diego Jacobs School of Engineering, La Jolla, California, USA. E-mail: sifraley@ucsd.edu*

†Electronic supplementary information (ESI) available. See DOI: 10.1039/c8bm01188e

‡These authors contributed equally.

We show that 8 kDa PEG can be used to fine-tune collagen architecture while simultaneously embedding cells, with no significant impact on cell viability, morphology, or migration. We also demonstrate that linearly increasing the amount of PEG added during collagen assembly and cell embedding reliably tunes fibril topography without significantly altering matrix stiffness or ligand density. Increasing amounts of PEG result in tighter networks of collagen fibers that are less degradable. This combination of features has the effect of confining cells in a rounded shape, reducing contractility, inducing the expression of cell–cell adhesion proteins, and triggering collective morphogenesis. We find that matrix degradability and fibril length are the strongest predictors of cellular confinement. In turn, confinement predicts collective cell behavior. This suggests that matrix degradability and fibril length are key biomaterial design features for tuning confinement and morphogenesis outcomes in collagen matrices.

## Results

### Macromolecular crowding with PEG tunes collagen fibrils

To explore the impact of collagen architecture on cancer cell behavior in a 3D matrix, we sought to tune the fibril network of a 2.5 mg ml$^{-1}$ collagen matrix without changing the density or stiffness of the matrix. The assembly of collagen I solution *in vitro* into a fibrous 3D matrix is thought to be driven by diffusion-limited growth of nucleated monomers, which is tunable through MMC.[29,30] Previous studies have used large molecular weight MMC agents (>50 kDa), which alter matrix stiffness along with fibril architecture.[24,25] We chose to use a lower molecular weight molecule (8 kDa) in an attempt to finely tune the fibril architecture and minimize impacts on mechanical properties of the matrix. In choosing our MMC material, we found that several agents have been shown to affect the proliferation or viability of cells.[31,32] However, PEG is a commonly used MMC agent for studies of biomolecular polymerization, like actin, and has been shown to be non-toxic for several different cell types including fibroblasts, cancer cells and stem cells.[33,34] Additionally, PEG is a widely used material for the preparation of hydrogels for the study of cell migration and morphogenesis programs.[35] Thus, we chose to test PEG for our purposes. First, we investigated whether 8 kDa PEG modulates the pre-nucleation and nucleation phases of collagen polymerization, as has been the reported effect of other MMC molecules on biopolymer fibrilation.[24,25] A dynamic turbidimetry analysis[24,36] (ESI Fig. 1A†) revealed that addition of PEG to collagen solutions during polymerization dramatically shortened the lag time before nucleation (ESI Fig. 1B†). This mechanism is similar to that of Ficoll and demonstrates that fibril architecture modification is a consequence of fibril formation in a molecularly crowded environment.[24]

Having validated PEG's ability to modify nucleation, we sought to tune collagen architecture. To do so, we introduced increasing amounts of 8 kDa PEG (0–10 mg ml$^{-1}$, labeled P0–P10) into a 2.5 mg ml$^{-1}$ collagen I solution during polymerization. The gels were then washed with PBS to remove the PEG. Fig. 1A shows the resulting fibril architecture. Based on the small hydrodynamic radius of 8 kDa PEG (2.45 nm[37,38]), we expected that diffusion of PEG out of the gel would not be hindered in any matrix condition. To validate this assumption, we measured the diffusivity of fluorescently labeled PEG in the matrix. We found no significant difference in the diffusion of PEG between the least and most crowded architectures (ESI Fig. 1C†). Additionally, SEM imaging of the P10 matrix showed no evidence of PEG after washing (Fig. 1B). These experiments indicate that the PEG included during polymerization is effectively removed by washing afterwards.

Next, we characterized the resulting collagen architectures (Fig. 1, A and B). Quantitative analysis of reflection confocal images after washing and removal of the PEG revealed a linear decrease ($r^2$ = 0.99, $p$ = 0.0005) in average fibril length from 14.1 μm without PEG (P0) to 11.7 μm with 8 mg ml$^{-1}$ of PEG (P8) mixed in during polymerization (Fig. 1C). Interestingly, this trend reversed between 8 and 10 mg ml$^{-1}$ of PEG, where average fibril length increased slightly from 11.7 μm to 12.4 μm (Fig. 1C). The average pore size of the matrices varied irregularly, ranging from 1.75 to 2.2 μm$^2$ (Fig. 1D). These measurements are consistent with those reported by other groups analyzing collagen matrices of similar density using confocal reflection microscopy (~0.78–1.8 μm$^2$ pore areas for 2.5 mg ml$^{-1}$ collagen;[39] 2–5 μm$^2$ pore areas for 1.7 mg ml$^{-1}$ (ref. 40)) and cryo-EM (~3 μm$^2$ pore areas, 2 mg ml$^{-1}$ collagen[41]). Since larger pores could be more relevant in terms of influencing cell behavior than the average pore size of the matrix, as large pores could allow for easier cell migration, we also analyzed the 99$^{th}$ percentile of pore size. Again, we found an irregular trend as crowding increases (Fig. 1E). Average fibril width, analyzed by SEM, varied by approximately 35 nm between the conditions with the highest and lowest PEG concentrations (ESI Fig. 1, D and E†). These data show that MMC with PEG tunes collagen matrix architecture, with an overall effect of producing tighter networks with shorter fibers and smaller pores.

### MMC does not significantly alter matrix mechanics

We next asked whether the mechanical properties of the 2.5 mg ml$^{-1}$ matrix changed as a function of fibril architecture. To assess this, we measured the bulk and local stiffness of each matrix using shear rheometry and atomic force microscopy (AFM), respectively, after washing out the PEG. No significant differences were observed in the bulk storage moduli across all conditions (P0–10) (Fig. 1F). To probe the local stiffness, an AFM tip of approximately the same size scale as nascent mechanosensory adhesions was chosen.[42] No significant differences were observed across all crowding conditions (Fig. 1G). Importantly, the non-significant variation in the measured stiffness is well below the reported threshold for mechanosensory cellular responses.[43,44] These experiments demonstrate that MMC modulates collagen fibril architecture without significant alterations to matrix stiffness.

 

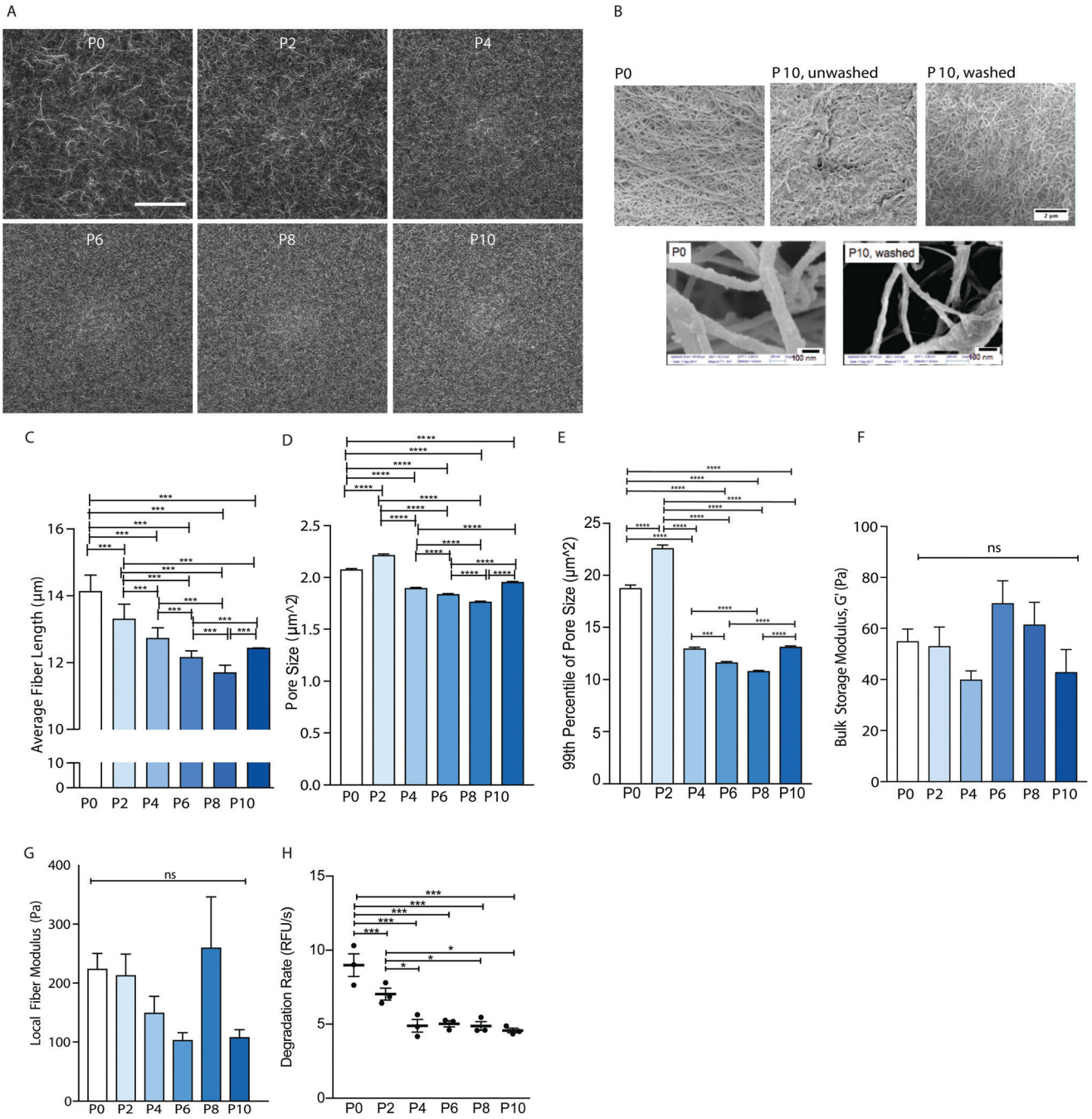


**Fig. 1** Fibril topography modulation by molecular crowding. (a) Reflection confocal micrographs of 2.5 mg $ml^{-1}$ collagen polymerized without a molecular crowding agent, P0, or with 2–10 mg $ml^{-1}$ of 8 kDa PEG as a crowding agent, P2–P10. Scale bar is 200 µm. (b) SEM images of a 2.5 mg $mL^{-1}$ collagen gel (top left) and 2.5 mg $ml^{-1}$ collagen gels polymerized with 10 mg $mL^{-1}$ PEG without washing (top middle) or with thorough washing before fixing (top right). Bottom images are magnified versions of top left and right images. (c) Characterization of mean fibril length as a function of the extent of crowding. (d) Characterization of mean pore size and (e) 99th percentile of pore size as a function of the extent of crowding. (f) Bulk storage moduli of control and crowded matrices measured by shear rheometry. (g) Local moduli of control and crowded matrices measured by AFM. Measurements were taken at multiple locations, ~10 fibrils per replicate, three replicates per condition. (h) Characterization of matrix degradability by rh-MMP-8 as a function of molecular crowding. Unless noted above, $n$ = 3 replicates per condition. At least three fields of view were analyzed per replicate. Graphs show the mean and standard error of measurements. Statistical significance tested by ANOVA and reported as $p < 0.001$, ***; $p < 0.01$, **; $p < 0.05$, *.

### MMC mediated fibril modification alters matrix degradability

Finally, we asked whether the degradability of the 2.5 mg ml$^{-1}$ matrix changed as a function of fibril architecture, since previous studies have shown a relationship between fibril architecture and sensitivity to enzymatic degradation.[24] To measure degradability, we incorporated dye-quenched (DQ) collagen into each matrix condition during gelation and MMC. After gelation, we removed the PEG using our washing procedure and added recombinant human MMP-8. Then, we monitored the rate of fluorescence increase, which corresponds to DQ collagen cleavage. Fig. 1H shows that increasingly crowded architectures corresponded to decreased degradability. To verify that diffusion of MMP-8 (52 kDa) was not hindered by changes in architecture, which could impact the rate of DQ cleavage, we measured the diffusivity of fluorescent dextran of approximately the same size (70 kDa) in the matrices. No significant differences in diffusivity were observed (ESI Fig. 1F†). Taken together, the results of our matrix characterization experiments show that MMC produces progressively tighter, less degradable collagen matrices without altering stiffness or total ligand density.

### MMC does not directly influence cell behavior

Our control experiments described above showed that PEG was not detectable in the matrices after washing. However, to ensure that potential residual PEG would not have a direct impact on cells, we conducted additional control experiments. We embedded MDA-MB-231 cells in a 2.5 mg ml$^{-1}$ collagen matrix with no PEG added during polymerization. Then, we added 10 mg ml$^{-1}$ PEG, the maximum concentration of PEG used in our matrix engineering experiments, on top of the fully polymerized matrix and allowed the 8 kDa molecules to freely diffuse into the interstitial spaces (Fig. 2A). In these experiments, no washing of the matrix was conducted. After 15 hours of culture, no significant differences were observed in cell morphology or migration, as assessed by cell circularity and the total path length traveled by the cells, respectively (Fig. 2, B and C). Next, we assessed the viability of the cells cultured for seven days in P0 gels with 10 mg ml$^{-1}$ PEG added after polymerization. Live-dead staining revealed a very slight increase in cell viability between the two conditions (Fig. 2, D and E). We also noted that cells remained as single cells during this week of culture with PEG (Fig. 2D). Reflection confocal analysis of the matrix architecture with and without PEG added after polymerization revealed only slight differences in average fibril length (<1 μm) and pore size (<0.5 μm$^2$) (ESI Fig. 2, B and C†). These control experiments confirm that residual PEG left by an imperfect wash does not alter cell morphology or influence the cell's ability to migrate.

### 3D collagen fibril topography patterns cell shape

Next, we explored the influence of matrix architecture on the morphology and migration of cancer cells. To do so, we polymerized 2.5 mg ml$^{-1}$ collagen I with a low seeding density of MDA-MB-231 breast cancer cells and 0–10 mg ml$^{-1}$ PEG mixed in. After polymerization, the cell-laden gels were washed to remove the PEG as described above. Single cells were then monitored using time lapse microscopy. Fig. 3A shows representative cell images observed at 15 h after seeding in each matrix condition. These morphology differences are a result of cell–matrix interactions as opposed to cell–cell interactions, as data was collected when cells were sparsely seeded and had not yet divided (ESI Fig. 2A†). Quantitative assessment of individual cell shapes at this 15 h timepoint revealed that cell circularity increases with increasingly crowded architectures (Fig. 3, A and B).

Based on prior studies by others in the field, which modified collagen architecture by varying gelation temperature and found that small pore sizes correlated with cell confinement, we hypothesized that small pores limited cell spreading and as such would be predictive of cell circularity. However, plotting pore size *versus* cell circularity revealed no significant correlation (ESI Fig. 2, D and E). However, plotting the mean fiber length against the mean cell circularity in each matrix condition (Fig. 3C) showed a strongly linear and significant inverse correlation ($r = -0.94$, $p = 0.005$). Likewise, plotting degradability of the matrix against the mean of cell circularity in each condition (Fig. 3D) also showed a strongly linear and significant inverse correlation ($r = -0.89$, $p = 0.02$). This suggests that both fiber length and degradability are covariates in MMC-engineered collagen architectures and are strong predictors of cell confinement.

### Confinement impacts cell contractility

Cell circularity induced by other means, *e.g.* microcontact ECM patterning or low stiffness substrates, is often associated with lower actomyosin contractility measured by reduced pMLC.[45,46] To probe the influence of confining matrix architecture on the contractile phenotype of cells, we blotted for pMLC 15 h post cell embedding. Cells in confining P10 matrices remained rounded and contained less pMLC, while those in non-confining P0 matrices had spread and contained more pMLC (Fig. 3E), indicating that confined cells were indeed less contractile.

### 3D collagen fibril topography modulates a transition from individual to collective cell behaviors and morphogenesis

Prior studies indicate that changes in actomyosin contractility can be associated with cellular reprogramming.[46] Therefore, we examined the impact of collagen fibril topography on breast cancer cell migration using the PEG-tuned matrices. To do so, we monitored MDA-MB-231 cells for seven days in P0–P10 matrix constructs. A striking transition from single cell behavior to collective morphogenesis was observed in the 2.5 mg ml$^{-1}$ collagen matrices crowded with at least 6 mg ml$^{-1}$ of PEG (P6, Fig. 4A). Collective cell behaviors arose in this condition as a series of distinct cell bodies in a chain-like structure. In the P8 and P10 conditions, similar chain-like structures were present, but were more fused and smooth-edged. These smooth-edged structures are characterized by having

 

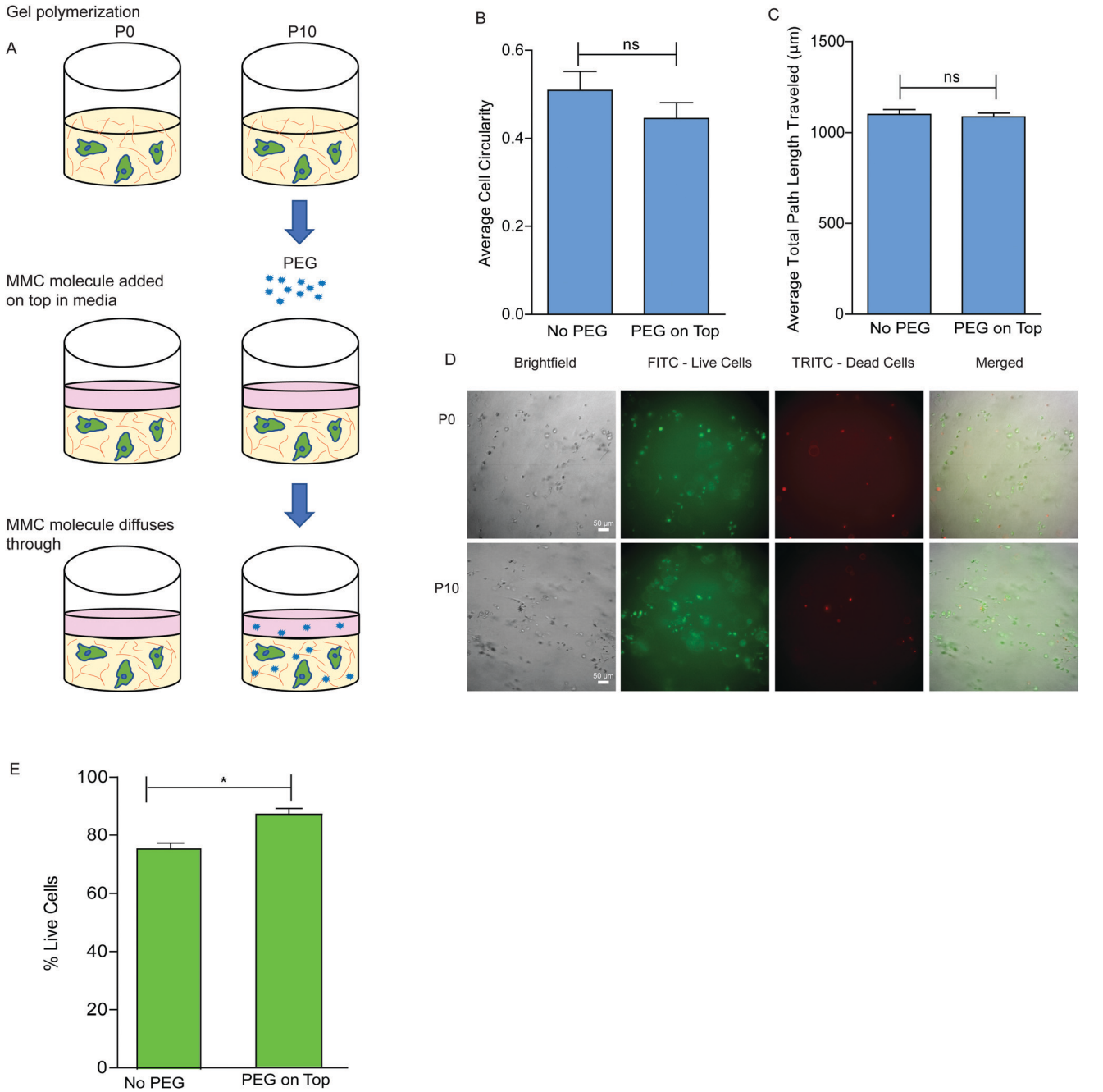


**Fig. 2** Influence of PEG alone on cell morphology, migration, and viability in 3D. (a) Schematic of control experimental setup. PEG was added *after* collagen polymerization to evaluate potential effects on cell behavior independent of matrix changes. Influence of PEG crowding on (b) cell circularity and (c) cell migration over 15 h. (d) Representative micrographs of cells after one week in culture showing brightfield (left), live (green), and dead (red) cell staining. Merged image on right. (e) Viability evaluated after one week of PEG crowding *after* polymerization. $N = 3$ biological replicates for each condition. At least 100 cells were analyzed per condition, ~35 per replicate. Bar graphs show the mean and standard error of measurements. Statistical significance tested by ANOVA and reported as $p < 0.001$, ***; $p < 0.01$, **; $p < 0.05$, *.

multiple cell bodies tightly fused to each other, with no apparent cellular protrusions extending outside the main structure (Fig. 4A and 5C). Fig. 4B shows the frequency of single cell, multicellular chain, and multicellular smooth structure phenotypes across all conditions. Multicellular structures resembling lobular and glandular structures of normal breast tissue[47] also emerged in the P8 and P10 conditions (Fig. 4C). Importantly, in the previously mentioned control condition where PEG was added after polymerization of a P0 matrix and left for seven days, no multicellular structures were observed (Fig. 2D). Again, this demonstrates that matrix architecture, not PEG, influences cell morphogenesis in our system.

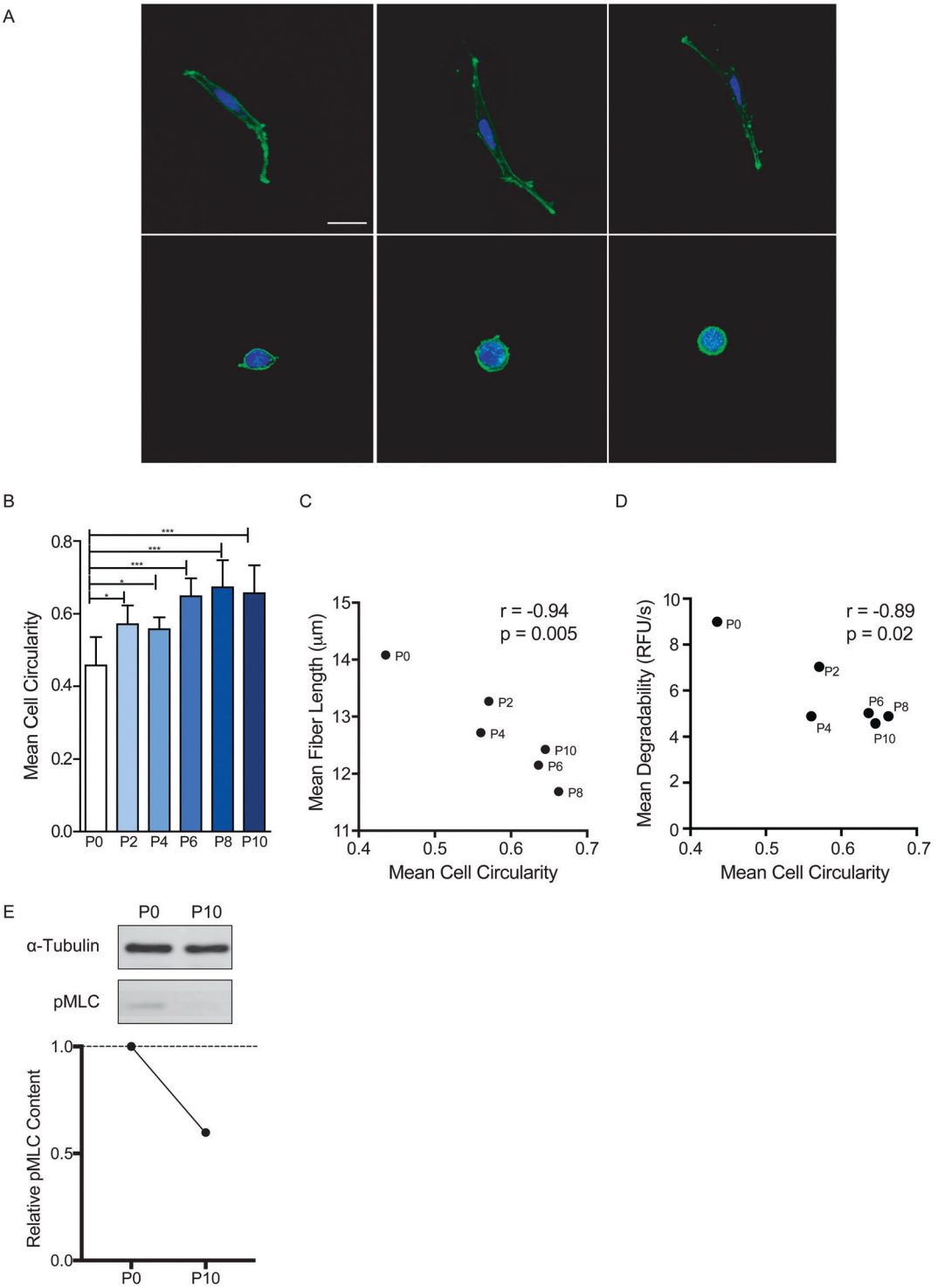


**Fig. 3** Influence of crowded collagen fibril architectures on cell shape. (a) Representative micrographs of cells in each matrix condition, P0–P10, after 15 hours showing phalloidin (actin, green) and DAPI (nuclei, blue). Scale bar is 25 μm. (b) Mean cell circularity of cells in each matrix construct. (c) Mean fiber length and (d) mean degradability plotted against mean cell circularity in each construct with Pearson correlation coefficient displayed and significance displayed. (e) Western blot analysis of phosphorylated myosin light chain (pMLC) of cells in 2.5 mg $ml^{-1}$ collagen (P0) and 2.5 mg $ml^{-1}$ collagen with 10 mg $ml^{-1}$ PEG (P10) at 15 h after embedding. $N = 3$ biological replicates for each condition. At least 100 cells were analyzed per condition, ~35 per replicate. Bar graphs show the mean and standard error. Statistical significance tested by ANOVA and reported as $p < 0.001$, ***; $p < 0.01$, **; $p < 0.05$, *.

 

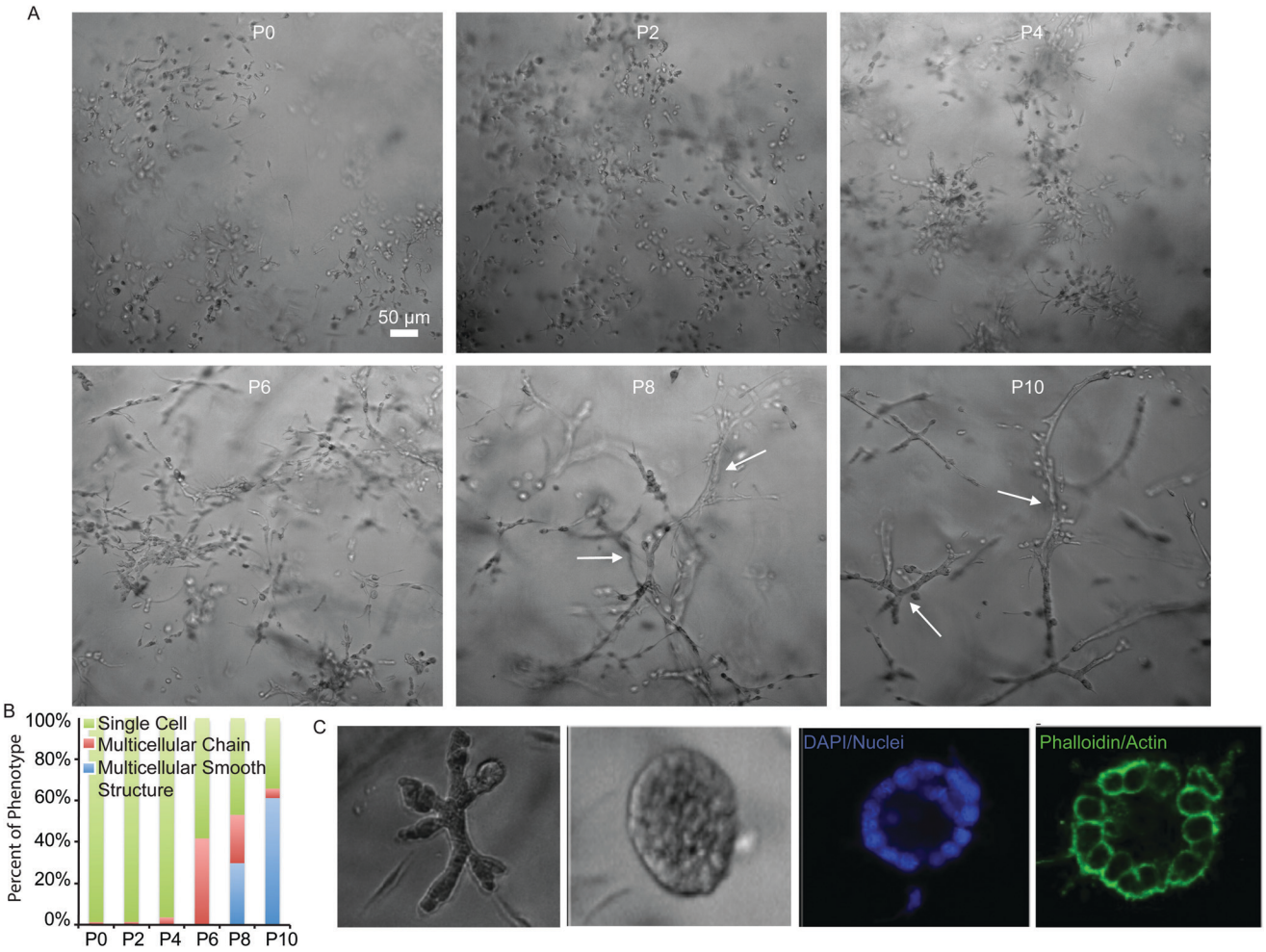


**Fig. 4** Influence of 3D fibril topography on cell behavior. (a) Representative brightfield micrographs of cells in each matrix construct after one week of culture. Arrows indicate the multicellular smooth structure phenotype that arises in the P8 and P10 conditions. (b) Frequency of phenotypes observed in each matrix construct. (c) Additional multicellular structures observed at low frequency in P8 and P10 conditions. Lobular (left) and acinar (right three images) structures resembling normal breast structures. Rightmost two images show representative acinar structure stained with DAPI (nuclei, blue) and phalloidin (actin, green), revealing an organized and hollow morphology.

Since tighter matrix architectures inhibited cell spreading and reduced pMLC at early timepoints (Fig. 3E), we wondered if matrix-induced cell confinement was predictive of the collective morphogenesis behaviors that arise later, over the course of seven days. To assess this, we compared cell circularity to the frequency of single cell *versus* multicellular phenotypes across the matrix conditions (Fig. 5A). We observed that multicellular structure formation was triggered exclusively in matrices where cell circularity was above ~0.6. As previously mentioned, cell circularity is predicted by matrix degradability and fiber length. This suggests that these two biomaterial parameters are useful for tuning single *vs.* collective behaviors through confinement.

To begin to elucidate the mechanism by which cells initiate cell–cell interactions in confining matrix architectures, we conducted gene expression analysis using RT-qPCR. This revealed that the multicellular phenotype is associated with expression of several cell–cell adhesion genes, including PECAM1, ICAM1, CTNNA1, ITGB4, and ITGB5 (Fig. 5B). Immunofluorescent staining of ICAM1 confirmed high protein expression in cell–cell junctions of MDA-MB-231 cancer cells undergoing the collective phenotype (Fig. 5C).

## Discussion

Using PEG as an MMC agent, we successfully tuned 3D collagen fibril architecture without significantly altering matrix stiffness or ligand density. The slight variation in the measured stiffness across crowding conditions was well below the reported threshold for mechanosensory cellular responses,[43,44] and is thus biologically insignificant. The stiffness of 2.5 mg ml$^{-1}$ collagen (P0) has previously been shown to mimic normal breast tissue.[9] All of our PEG-crowded and non-crowded 2.5 mg ml$^{-1}$ collagen constructs are within this range of stiffness and can be considered representative of

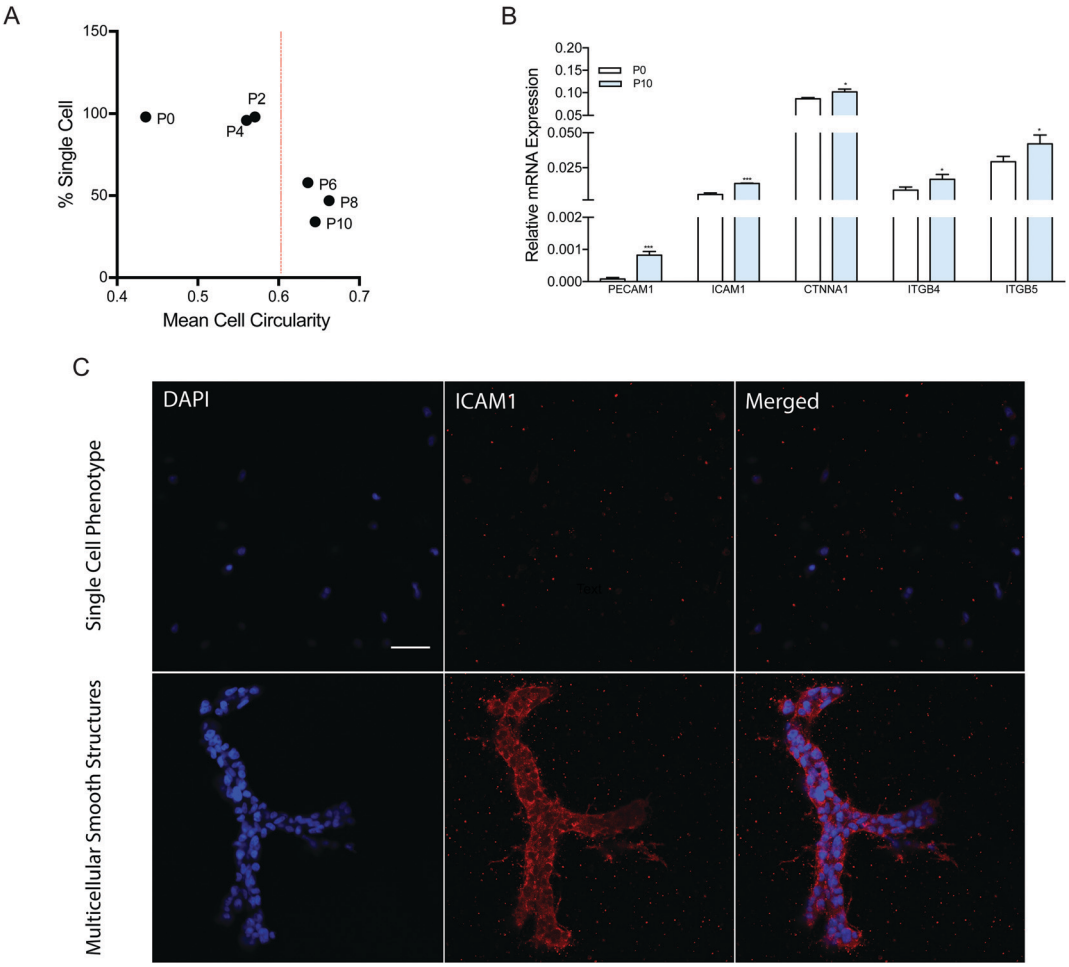


**Fig. 5** Cell confinement within the matrix predicts collective behavior. (a) Frequency of the single cell phenotype in each matrix construct plotted against the mean cell circularity in each construct. Red line shows the approximate cell circularity threshold predicting the transition from single to multicellular behavior. (b) Relative mRNA expression of cell–cell adhesion genes upregulated by cells in P10 constructs. (c) Immunofluorescence staining of MDA-MB-231 cells undergoing the multicellular phenotype. DAPI (nuclei, blue), ICAM1 (red), and merged images are shown. Scale bar shows 100 μm. $N = 3$ biological replicates for each measurement. Statistical significance tested by ANOVA and reported as $p < 0.001$, ***; $p < 0.01$, **; $p < 0.05$, *.

the mechanical conditions cancer cells encounter during tissue invasion and metastasis.

The magnitude of the architectural changes induced by crowding were not as dramatic as those previously achieved by other means, such as varying gelation temperature or using larger MMC agents. This may explain the similarity in the mechanical behavior among our different collagen architectures created using a small MMC, whereas changes induced by larger MMCs or gelation temperature variations are greater and do impact matrix mechanics.[16,40] The similarity in mechanical properties across our crowding conditions may result from a balance between an increase in the connectivity of the collagen network (shorter fibers, smaller pores) and a simultaneous weakening of fibril connections, since overall density does not change.[48] Despite the relatively small magnitude of changes in matrix architecture produced by MMC, these were significant enough to dramatically alter cell behavior.

Similar to other MMC agents, our data shows that PEG causes a significant decrease in the lag time during the nucleation phase of collagen I gelation, thus leading to the development of shorter fibers. Interestingly, we show that this change can be achieved using a relatively small molecule (8 kDa) as compared to previous reports where molecules up to 400 kDa have been used. The fractional volume occupancy (FVO) we achieve with 8 kDa PEG is comparable to that achieved in previous studies using Ficoll and other larger macromolecules. For example, Raghunath's group previously showed that a FVO of 8.06% 400 kDa Ficoll in Collagen I gels was enough to alter matrix assembly.[24] Using the same FVO calculation we estimate that we achieve a 4.63% FVO with 10 mg $mL^{-1}$ of 8 kDa PEG, the maximum concentration of PEG used in our matrix engineering experiments. We calculated FVO using the hydrodynamic radius of PEG 8000 as 2.45 nm.[38] The hydrodynamic radius is the preferred measurement when considering excluded volume effect of soluble macromolecules.[31] However,

 

it is also important to note that we use a higher concentration of collagen in our gels (2.5 mg $mL^{-1}$) than was used in previous reports (0.8 mg $mL^{-1}$), which is expected to contribute to self-crowding of the collagen.[24] These observations suggest that when MMC is used for 3D ECM architecture tuning, MMC size and FVO as well as ECM molecule size and FVO should be considered in an application-dependent manner. PEG and other MMCs have also been used as precipitating agents and to support deposition of ECM by cultured cells.[27] To minimize these effects, which were undesired in our study, we thoroughly removed excess PEG in the collagen gels immediately after polymerization.

Increasing amounts of PEG linearly tuned fibril length until at high PEG concentration, where this trend reversed. The degradability of the matrices also decreased linearly with crowding, then plateaued. Non-linear polymerization effects at high PEG crowding concentrations have also been observed for actin filaments, where bundling is induced when the concentration of PEG exceeds a critical onset value.[49] Studies have shown that PEG polymers are not always excluded in a way that fits the hard-sphere model of crowding,[50] and a wide range of partial exclusion as a function of concentration is possible.[51] This may explain the non-linear collagen polymerization behavior we observed at high concentrations of PEG. In addition to concentration, the chemical nature of an MMC agent as well as its size can determine its exclusion from molecular surfaces, so MMC chain size and chemistry could be two additional "tuning knobs" to systematically explore for matrix engineering purposes.

Fibril length and matrix degradability were both linearly and significantly predictive of the degree to which cells were confined by the matrix, as measured by cell circularity index. However, pore size varied irregularly as crowding was increased and was not significantly correlated with cellular confinement. This may appear surprising because another study, which used gelation temperature to modulate collagen architecture, found a linear correlation between pore size and cell confinement.[40] However, this study did not assess whether matrix degradability was also altered as a function of changing gelation temperatures. When modifying collagen architecture through polymerization temperature, pore size and degradability may be covariates. Degradability dictates the cell's ability to modify the matrix and expand the pore size locally with MMPs, making initial pore size quickly irrelevant in a degradable matrix. Degradability is also required for integrin binding on 2D matrix-coated substrates.[52] If this is true for 3D fibril matrices, then cells may remain rounded in low-degradability matrices because they are unable to adhere, not because of steric confinement by small pores. In future work, we plan to examine how matrix degradability influences cell adhesion in our 3D collagen system.

Our results suggest that in native collagen matrices, degradability is a biomaterial feature that predicts cell confinement and thereby cell fate. These findings are consistent with studies showing that the degradability of synthetic hydrogels directs stem cell fate.[53,54] In our study, the degree of cell confinement induced by matrix architecture modulated actomyosin contractility and predicted distinct modes of cancer cell migration and gene expression. Single cell migration was favored in non-confining matrices where pMLC was initially high, whereas multicellular migration and morphogenesis was favored in confining matrices where pMLC was initially low. The multicellular chain phenotype we observe in our P6 construct is similar to a phenotype observed in fibrosarcoma and melanoma cells in high density collagen matrices, where individual cell bodies are distinguishable but touching, resembling a pearl necklace.[16,55] However, the fused networks, glands, and lobule structures formed in our P8 and P10 conditions are distinct. Weaver and colleagues previously reported the reversion of a malignant breast cancer cell line into a normal glandular phenotype through the blockade of integrin beta 1 (ITGB1), which inhibits adhesion to the ECM substrate.[56] As discussed above, low degradability matrices could also limit adhesion[52] and as such could impinge on the same pathways to induce collective morphogenesis behaviors. Interestingly, less degradable forms of collagen I are deposited in many cancers, fibrotic tissues, and during embryogenesis.[57] This could function to confine cells *in vivo*. Alternatively, physical confinement of cells in a rounded shape could alter the tensegrity of the cell, reducing the activation of cell surface integrins and their affinity for binding ECM.[58,59]

We identified that the cell–cell adhesion genes PECAM1, ICAM1, CTNNA1, ITGB4, and ITGB5 were upregulated by breast cancer cells undergoing morphogenesis induced by confining matrices. ICAM1 expression in cancer cells has been correlated with more aggressive tumors and has been shown to mediate survival, migration, extravasation, homing, and metastasis.[60–62] However, it is not fully understood how ICAM1 expression is regulated in cancer.[63] Our study shows that 3D collagen architecture regulates ICAM1 expression. Confining architectures likely induce this gene expression program through the alterations to actomyosin contractility that we observed,[59,64–68] however more work is necessary to identify the molecular mechanisms.

It will also be important to identify what drives the development of the heterogeneous structures formed by the breast cancer cells in our system and whether these represent different metastatic capabilities. The more abundant network phenotype we observe is reminiscent of the collective migration pattern implicated as the primary mode of tumor cell dissemination.[69,70] This collective invasion behavior is thought to be linked to circulating tumor cells that are present as aggregates, which are predictive of poorer clinical outcomes.[55,71,72] Thus, collagen architecture and confinement in the tumor microenvironment may influence the metastatic capabilities of cancer cells through modulation of migration phenotype and cell–cell adhesion protein expression.

## Conclusions

MMC is a robust technique to modify collagen fibril architectures in 3D hydrogels. Here we built on previous studies to

develop an MMC technique for tuning 3D collagen architecture without significantly altering stiffness. This led us to discover an association between matrix degradability and cellular confinement, leading to low actomyosin contractility and cellular reprogramming into a collective morphogenesis phenotype. We propose that MMC-mediated modification of collagen fibrils represents a powerful biomaterials technique to develop physiologically relevant *in vitro* models to study cancer cell biology.

A deeper understanding of the microenvironmental regulators of cancer cell migration could help identify therapies to combat metastasis and improve patient outcomes. By tuning collagen architecture in a way that decouples matrix architecture from density and stiffness, our study adds support for the strong role of ECM degradability and cellular confinement in modulating cancer cell behavior. The same techniques could be extendable to investigations of metastatic migration *in vivo*, since our 3D matrix constructs are implantable. These techniques may also be useful for stem cell and regenerative medicine studies as a means to control 3D morphogenesis outcomes in a native ECM.

# Methods

### Cancer cell culture

MDA-MB-231 breast cancer cells were ordered from ATCC (Manassas, VA) and cultured in Dulbecco's Modified Eagle's Medium (Life Technologies, Carlsbad, CA) supplemented with fetal bovine serum (Corning, Corning, NY) and gentamicin (Life Technologies, Carlsbad, CA), at 37 °C and 5% $CO_2$. Culture media was changed every other day as needed. Cells were cultured to 80% confluence prior to being trypsinized and embedded inside of 3D collagen I matrices at a seeding density of 50 000 cells per gel. Cell laden gels were cultured for a week to observe long-term phenotypic differences, with media changes every other day.

### 3D culture in collagen I matrix

High concentration, rat tail acid extracted type I collagen was ordered form Corning (Corning, NY). MMC agent PEG 8000 (8000 Da) was ordered in powder form from Sigma-Aldrich (St Louis, MO) and reconstituted in PBS (Life Technologies, Carlsbad, CA) immediately before usage. Trypsinized cells to be embedded, were first mixed with 1× reconstitution buffer composed of sodium bicarbonate, HEPES free acid, and nanopure water. Appropriate amounts of MMC agent were then added to produce final concentrations of 0, 2, 4, 6, 8, and 10 mg $ml^{-1}$ PEG (denoted by P0, P2, P4, P6, P8, P10). Afterwards, collagen solution was added to the mixture for a final concentration of 2.5 mg $ml^{-1}$ collagen. Finally, pH of the final mixture was adjusted using 1 N sodium hydroxide, prior to polymerization *via* incubation at 37 °C (~1 h). Gels were prepared inside of 48-well plates with a total volume of 200 µl. Following gel polymerization, MMC molecules were washed out of the collagen gels by rinsing with PBS 3× for 5 min each. Cell culture media was then added on top of the gels and changed every two days.

### Turbidimetry assay

Collagen I turbidimetric analyses were performed as done by Dewavrin *et al.* Solutions of collagen I were prepared at 2.5 mg $ml^{-1}$ with and without the addition of 10 mg $ml^{-1}$ PEG, and immediately transferred to a 96-well plate pre-heated to 37 C for polymerization in a Tecan Infinite 200 Pro (Tecan, Männedorf, Switzerland) at the stem cell core of Sanford Consortium of Regenerative Medicine (La Jolla, CA). The plate temperature was maintained at 37 C for 600 seconds (until the plateau phase was established) while absorbance was recorded every 7 seconds at 313 nm. Lag time before nucleation was calculated as the *x*-intercept of a line tangent to the linear growth phase ($R^2 = 0.99$).

### Degradation assay

In order to measure degradation by matrix metalloproteinase 8 (MMP8), 3D Collagen I-DQ matrices were formulated as previously described. Recombinant human MMP–8 (rhMMP-8) (R&D Biosystems, Catalog #908-MP) was activated at 100 µg $mL^{-1}$ with 1 mM *p*-aminophenylmercuric acetate (APMA) (Sigma, Catalog #A-9563) in TCNB Assay Buffer at 37 °C for 1 hour. Following incubation, activated rhMMP-8 was diluted to 1.0 ng $\mu L^{-1}$ in TCNB assay buffer and was added on top of each of the gels to a final concentration of 0.45 µg $mL^{-1}$. Immediately after MMP8 exposure, fluorescence was measured using a Tecan Infinite 200 Pro (Tecan, Männedorf, Switzerland) at the stem cell core of Sanford Consortium of Regenerative Medicine (La Jolla, CA). Fluorescence was measured at excitation (488 nm) and emission (525 nm) wavelengths over a kinetic cycle of 13 hours, with 2-minute intervals.

### MMC control experiments

To ensure that the MMC agent PEG was truly inert, we investigated its potential effects separate from changes in matrix architecture. For these experiments, MDA-MB-231 cells were embedded inside of 2.5 mg $ml^{-1}$ collagen gels. After the gels were polymerized, culture media containing 10 mg $ml^{-1}$ PEG was added on top. The MMC molecules were left in the media and allowed to diffuse down into the gel containing the cells. Subsequent media changes also included appropriate amounts of MMC agent to maintain the PEG and concentration in the gel for the week long experiment.

### Time lapse imaging microscopy

Time lapse microscopy was conducted using a Nikon Ti-E inverted microscope, equipped with a stage top incubation system. Time-lapse imaging began at around the $8^{th}$ hour after the cells were embedded into the collagen gels. For motility, proliferation, and circularity analyses, each gel was imaged at 10× over 6 fields of view (FOV) for a period of 15 h, with images being taken every 2 min.

 

### Cell proliferation assay

Cell viability was assessed using a Live and Dead Cell Assay (Abcam, Cambridge, UK). Intact, viable cells fluoresce green (imaged under FITC channel) while dead cells fluoresce red (imaged under TRITC channel). The average number of live cells, dead cells, and live cell viability percentages were calculated over 4 FOVs per condition. Live cell viability % is defined as the number of live cells/the total number of cells × 100.

### Confocal reflection microscopy and matrix analysis

Collagen matrix architecture and topography were investigated by imaging gels using confocal reflection microscopy (CRM) with a Leica SP5 inverted confocal microscope. The microscope was equipped with a 20× immersion objective (NA = 1.0). Collagen fibrils were imaged by exciting with and collecting backscattered light at 488 nm. Confocal reflection imaging is restricted to fibrils that are oriented within 50° of the imaging plane.[73]

All matrix analyses were done using CRM images (fiber length and pore size) and SEM images (fiber width) of the collagen gels in each condition over 3 FOVs per biological triplicate. Fibril analysis was conducted in CT-FIRE v1.3 by measuring individual fibril length and width as previously published.[74] Minimum fibril length, dangler length threshold (thresh_dang_L), short fibril length threshold (thresh_short_L), distance for linking same-oriented fibrils (thresh_linkd), and minimum length of a free fibril (thresh_flen), were all set to three pixels. Default settings were used for all other fibril extraction parameters and output figure controls. Settings were optimized to detect and analyze discrete fibrils in CRM images on scales of 0.72 μm per pixel. Examples of the fibrils found by CT-FIRE are shown in ESI Fig. 3D,† along with the associated reflection confocal micrographs.

Pore size was calculated using NIS-Elements software (Nikon) as the 2D area encompassed by fibrils. The total pore area ($\varepsilon'$) as a 2D approximation of the 3D tissue ultrastructure ($\varepsilon$) can be described as:

$$\varepsilon' = \varepsilon \exp\left(\frac{-\alpha D_f}{4\varepsilon}\right) \quad (1)$$

as long as the stereological assumption is met.[75] To verify this assumption, we imaged them from the top and from one of the sides (*XY* and *YZ* planes) using the same imaging settings. ESI Fig. 3A and B,† show that differences in fibril length were negligible. ESI Fig. 3C† shows that a small difference in pore size was detected (<0.5 $\mu m^2$ difference). However, this difference is less than the pixel size (0.52 $\mu m^2$ per pixel).

Additionally, if the imaging depth of field ($D_f$) is small enough $\varepsilon' = \varepsilon$. We calculate our $D_f$ from:

$$D_f = \frac{\lambda n}{NA^2} + \frac{n}{M \cdot NA} e \quad (2)$$

to be ~0.67 microns. This is smaller than the pixel size in our system and smaller than the expected $\varepsilon$, which makes the fraction in eqn (1) <1 and suggests that $\varepsilon' \cong \varepsilon$ is a valid approximation. These analyses suggest that our 2D confocal micrographs are a sufficiently close representation of the 3D architecture.

Pre-processing of images were conducted by implementing a Gauss-Laplace Sharpen set to a power of 2 and then by using a Rolling Ball Correction with a rolling ball radius of 15.[76] The contrasts of all images were equalized, then images were binarized by thresholding to the same range. Next the automated measurement tool was used to measure pore areas in the binarized images. Single pixel pore values were attributed to speckle noise and removed from all conditions.

### Rheometry

Rheological measurements were conducted following established protocols[77] using a hybrid rheometer (DHR-2) from TA Instruments (New Castle, DE). 610 μL PEGylated collagen gels were measured on a cone and plate geometry with a 53 μm gap. Gels were allowed to polymerize in contact with the cone and plate in a humidified incubation chamber for 30 minutes at 37 °C before measurement. For each condition, a strain sweep at frequency of 1 rad $s^{-1}$ was recorded to determine each gel's viscoelastic region. The storage modulus ($G'$) and loss modulus ($G''$) were recorded over frequencies of 0.1–100 rad $s^{-1}$ within the linear region (0.8%). The storage modulus ($G'$) at 100 rad $s^{-1}$ was reported for each condition. Three independent replicates were performed for each condition tested.

### Atomic force microscopy (AFM)

AFM was performed to measure local collagen gel stiffness as previously described.[78–81] Briefly, nano-indentations were performed using a MFP-3D Bio Atomic Force Microscope (Oxford Instruments) mounted on a Ti-U fluorescent inverted microscope (Nikon Instruments). A pyrex-nitride probe with a pyramid tip (nominal spring constants of 0.08 N $m^{-1}$, 35° half-angle opening, and tip radius of 10 nm, NanoAndMore USA Corporation, cat # PNP-TR) was first calibrated for the deflection inverse optical lever sensitivity (Defl InvOLS) by indentation in PBS on glass followed by using a thermal noise method provided by the Igor 6.34A software (WaveMetrics) as previously described.[78] Samples were loaded on the AFM, submersed in phosphate buffered saline (PBS), and indented at a velocity of 2 μm $s^{-1}$. Samples were indented until the trigger point, 2 nN, was achieved. Five measurements, equally spaced 50 μm apart, were taken per gel. Tip deflections were converted to indentation force for all samples using their respective tip spring constants and Hooke's Law. Elastic modulus was calculated based on a Hertz-based fit using a built-in code written in the Igor 6.34A software. The Hertz model used for a pyramidal tip is:

$$F = \frac{2}{\pi} \tan(\alpha) \frac{E}{1-\nu^2} \delta^2 \quad (3)$$

where $F$ is force, $\alpha$ is the half-angle opening of the tip, $\nu$ is the Poisson's ratio, $E$ is elastic modulus and $\delta$ is indentation. We assumed a Poisson's ratio of 0.5 (incompressible) for all

samples. Curves were only analyzed if at least 80% of the fit curve crossed over the data points. ESI Fig. 4A† shows force-position plots of raw data where the calculated indentation points are indicated and aligned between soft (blue) and stiff curves (red). When the indentation force trigger was met, *e.g.* when the probe is centered over a pore, data is not collected. ESI Fig. 4B† plots an example of the force curve (orange) that would be obtained from a pore, noting that there is no calculable contact point and tip deflection is only the result of drag on the cantilever during tip approach.

### Scanning electron microscope (SEM)

Collagen gels were prepared at 2.5 mg $mL^{-1}$ concentration with and without the addition of 10 mg $mL^{-1}$ 8 kDa PEG, then placed in a humidified incubator (37 °C) until fully polymerized as described above. The samples polymerized in the presence of PEG were separated into washed and not washed preparations. To wash the PEG after polymerization, PBS was added on top of the gel and placed in the incubator for 5 minutes 3 times. Next, all samples were fixed with 4% PFA for 1 hour at room temperature and the washed 3× with PBS. The samples were then dehydrated by treating them with increasing concentrations of ethanol (50% to 100%). Samples immersed in 100% ethanol were subjected to critical point drying (Autosamdri-815, Tousimis, Rockville, MD, USA), coated with a thin layer of Iridium (Emitech K575X, Quorum technologies, Ashford, UK) and imaged using a Zeiss sigma 500 SEM. Gels were cut with a razor blade to expose cross-sections of the material for imaging.

### Diffusivity analysis

To analyze the penetration of the PEG crowding agent into the 3D collagen matrices, we conducted diffusion experiments through gels polymerized in microchannels (μ-Slide VI 0.4, IBIDI, Munich, Germany). Collagen gels were prepared as described above and polymerized inside the microchannel for 1 hour at 37 °C. Subsequently an 88 μM solution of 70 kDa fluorescein-conjugated dextran or a 0.31 mM solution of fluorescein-conjugated 8 kDa PEG were added to one end of the microchannel while the equivalent volume of cell growth medium was added to the other end. The microchannel was then imaged in a fluorescent microscope at 1 min intervals for 8.5 hours to track the solute diffusion through the collagen matrix. Images were analyzed using ImageJ and a concentration profile was determined for each time point. The data was fitted to Fick's Second Law for 1-D diffusion (eqn (4)), and the diffusion coefficient, $D$, was determined for runs with an $R$-squared value of greater than or equal to 0.90.

$$C(t, X) = C_{\max} \times \left(1 - \operatorname{erf}\left(\frac{X}{2\sqrt{Dt}}\right)\right) \quad (4)$$

where $C_{\max}$ is the initial concentration at the source, erf is the error function, $X$ is length, and $t$ is time.

### Cell analysis

Individual cells in the time lapse videos were tracked in Metamorph for motility characterization. Within the 15 h time lapse window, cells were analyzed in terms of the total path length traveled, their average speed, the invasion distance (displacement), and the persistence of their migration (defined as the invasion distance/the total path length traveled). Cell morphology analysis was conducted using images of the cells during the $11^{th}$ and $15^{th}$ hour after seeding in the gel, in terms of circularity:

$$\text{Circularity} = \frac{4\pi A}{P^2} \quad (5)$$

where $A$ is the cross-sectional area and $P$ is cross-sectional perimeter of the cell.

### Correlation analysis

Correlations were calculated in terms of the Pearson correlation coefficient using GraphPad software.

### RNA isolation and purification

Three independent replicates of 3D collagen I gels were seeded at 50 000 cells per gel per condition tested. RNA was harvested after 7 days by gel homogenization in TRIzol reagent (Thermofisher, Waltham, MA). Total RNA was isolated using a chloroform extraction according to manufacturer's instructions. RNA was subsequently purified using High Pure RNA Isolation Kit (ROCHE, Branford, CT).

### Gene expression analysis by qPCR

Following the RNA extraction, cDNA was synthesized using the SuperScript III First-Strand Synthesis System (Thermofisher, Waltham, MA). The TaqMan Array Human Extracellular Matrix & Adhesion Molecules 96-well Plate was utilized to identify genes of interest (Thermofisher, Waltham, MA). Relative mRNA levels were quantified by calculating the ΔCt using ACTB as a reference gene.

### Statistics

Data presented in bar graph format was analyzed using one-way analysis of variance (ANOVA) followed by Tukey or Newman–Keuls *post hoc* test in GraphPad Prism (v5). Correlation plots were analyzed by Pearson Correlation in GraphPad Prism (v5). Pearson $r$ correlation coefficient and two-tailed $p$ values are reported. $N = 3$ biological replicates for each condition tested. Statistical significance was reported as $p < 0.001$, ***; $p < 0.01$, **; $p < 0.05$, *.

### Western blotting from 3D constructs

200 μL 3D collagen constructs were scooped out of their wells into vials containing 1 mL of PBS and immediately spun down at 1500*g* for 5 min. Supernatant per vial was discarded and 200 μL of Pierce IP Lysis Buffer containing proteases and phosphatase inhibitor cocktails was added to the pellets (Thermofisher Scientific, Waltham, MA). Loading buffer con-

 

taining SDS and DTT was added to achieve a final 1× concentration. The samples were then sonicated on ice for 30 s, then boiled at 95 C for 5 min. Proteins were separated by SDS-PAGE and transferred to a PVDF membrane. Membranes were then probed with antibodies against phosphorylated myosin light chain (Cell Signaling Technology, Danvers, MA) and alpha Tubulin (TU-01, Thermofisher).

## Author contributions

S.R., R.M., A.H., D.O.V., and S.F. designed the study. S.R. and R.M. conducted rheometry and cell–cell adhesion experiments. S.R., R.M., and D.O.V conducted diffusivity and degradability experiments. S.R. and A.H. conducted all other matrix characterization experiments. D.O.V. conducted SEM experiments. S.R. and A.K. conducted AFM experiments. A.H. conducted PEG control experiments and collective cell migration experiments. D.O.V. and S.R. conducted all other supplementary data experiments. All authors contributed to writing or editing the manuscript.

## Data availability

All relevant data is available within the article and supplementary files, or from the corresponding author upon request.

## Conflicts of interest

The authors declare no competing interests.

## Acknowledgements

We thank Dr Pedro Cabrales for use of his rheometer. We thank members of the Fraley lab for their technical assistance and insightful comments regarding this work. We thank NSF REU student Tyler Goshia for his assistance in preliminary studies of collagen crowding.

S. F. and lab is supported by a Burroughs Wellcome Fund Career Award at the Scientific Interface (1012027), NSF CAREER Award (1651855), ACS Institutional Research Grant (15-172-45-IRG) provided through the Moores Cancer Center, UCSD, and UCSD CTRI, FISP, and CRES pilot grants. Support was also provided by NIH grants (R01CA206880 to A. J. E.) and by fellowship support *via* NSF GRFP and NIH T32AR060712 (to A. K.).

## References

1 M. Fang, J. Yuan, C. Peng and Y. Li, Collagen as a double-edged sword in tumor progression, *Tumor Biol.*, 2014, **35**, 2871–2882, DOI: 10.1007/s13277-013-1511-7.

2 M. W. Conklin, *et al.*, Aligned collagen is a prognostic signature for survival in human breast carcinoma, *Am. J. Pathol.*, 2011, **178**, 1221–1232, DOI: 10.1016/j.ajpath.2010.11.076.

3 P. P. Provenzano, *et al.*, Collagen density promotes mammary tumor initiation and progression, *BMC Med.*, 2008, **6**, 11, DOI: 10.1186/1741-7015-6-11.

4 S. I. Fraley, Y. Feng, A. Giri, G. D. Longmore and D. Wirtz, Dimensional and temporal controls of three-dimensional cell migration by zyxin and binding partners, *Nat. Commun.*, 2012, **3**, 719, DOI: 10.1038/ncomms1711.

5 S. I. Fraley, *et al.*, A distinctive role for focal adhesion proteins in three-dimensional cell motility, *Nat. Cell Biol.*, 2010, **12**, 598–604, DOI: 10.1038/ncb2062.

6 X. Yue, J. K. Lukowski, E. M. Weaver, S. B. Skube and A. B. Hummon, Quantitative Proteomic and Phosphoproteomic Comparison of 2D and 3D Colon Cancer Cell Culture Models, *J. Proteome Res.*, 2016, **15**, 4265–4276, DOI: 10.1021/acs.jproteome.6b00342.

7 G. Jiang, A. H. Huang, Y. Cai, M. Tanase and M. P. Sheetz, Rigidity sensing at the leading edge through alphavbeta3 integrins and RPTPalpha, *Biophys. J.*, 2006, **90**, 1804–1809, DOI: 10.1529/biophysj.105.072462.

8 C. M. Lo, H. B. Wang, M. Dembo and Y. L. Wang, Cell movement is guided by the rigidity of the substrate, *Biophys. J.*, 2000, **79**, 144–152, DOI: 10.1016/s0006-3495(00)76279-5.

9 M. J. Paszek, *et al.*, Tensional homeostasis and the malignant phenotype, *Cancer Cell*, 2005, **8**, 241–254, DOI: 10.1016/j.ccr.2005.08.010.

10 K. Wolf, *et al.*, Physical limits of cell migration: control by ECM space and nuclear deformation and tuning by proteolysis and traction force, *J. Cell Biol.*, 2013, **201**, 1069–1084, DOI: 10.1083/jcb.201210152.

11 J. Xie, M. Bao, S. M. C. Bruekers and W. T. S. Huck, Collagen Gels with Different Fibrillar Microarchitectures Elicit Different Cellular Responses, *ACS Appl. Mater. Interfaces*, 2017, **9**, 19630–19637, DOI: 10.1021/acsami.7b03883.

12 G. C. Wood and M. K. Keech, The formation of fibrils from collagen solutions 1. The effect of experimental conditions: kinetic and electron-microscope studies*, *Biochem. J.*, 1960, **75**, 588–598.

13 D. Ceballos, *et al.*, Magnetically aligned collagen gel filling a collagen nerve guide improves peripheral nerve regeneration, *Exp. Neurol.*, 1999, **158**, 290–300, DOI: 10.1006/exnr.1999.7111.

14 A. L. Oliveira, *et al.*, Aligned silk-based 3-D architectures for contact guidance in tissue engineering, *Acta Biomater.*, 2012, **8**, 1530–1542, DOI: 10.1016/j.actbio.2011.12.015.

15 N. Dubey, P. C. Letourneau and R. T. Tranquillo, Neuronal contact guidance in magnetically aligned fibrin gels: effect of variation in gel mechano-structural properties, *Biomaterials*, 2001, **22**, 1065–1075.

16 A. Haeger, M. Krause, K. Wolf and P. Friedl, Cell jamming: collective invasion of mesenchymal tumor cells imposed by

tissue confinement, *Biochim. Biophys. Acta*, 2014, **1840**, 2386–2395, DOI: 10.1016/j.bbagen.2014.03.020.

17 A. Ray, Z. M. Slama, R. K. Morford, S. A. Madden and P. P. Provenzano, Enhanced Directional Migration of Cancer Stem Cells in 3D Aligned Collagen Matrices, *Biophys. J.*, 2017, **112**, 1023–1036, DOI: 10.1016/j.bpj.2017.01.007.

18 Y. N. Zeng, Y. L. Kang, L. R. Rau, F. Y. Hsu and S. W. Tsai, Construction of cell-containing, anisotropic, three-dimensional collagen fibril scaffolds using external vibration and their influence on smooth muscle cell phenotype modulation, *Biomed. Mater.*, 2017, **12**, 045019, DOI: 10.1088/1748-605X/aa766d.

19 M. Antman-Passig, S. Levy, C. Gartenberg, H. Schori and O. Shefi, Mechanically Oriented 3D Collagen Hydrogel for Directing Neurite Growth, *Tissue Eng., Part A*, 2017, **23**, 403–414, DOI: 10.1089/ten.TEA.2016.0185.

20 P. P. Provenzano, K. W. Eliceiri, D. R. Inman and P. J. Keely, Engineering three-dimensional collagen matrices to provide contact guidance during 3D cell migration, *Curr. Protoc. Cell Biol.*, 2010, DOI: 10.1002/0471143030.cb1017s47, ch. 10, unit 10.17.

21 A. J. Engler, *et al.*, Myotubes differentiate optimally on substrates with tissue-like stiffness: pathological implications for soft or stiff microenvironments, *J. Cell Biol.*, 2004, **166**, 877–887, DOI: 10.1083/jcb.200405004.

22 C. Chen, F. Loe, A. Blocki, Y. Peng and M. Raghunath, Applying macromolecular crowding to enhance extracellular matrix deposition and its remodeling in vitro for tissue engineering and cell-based therapies, *Adv. Drug Delivery Rev.*, 2011, **63**, 277–290, DOI: 10.1016/j.addr.2011.03.003.

23 R. R. Lareu, *et al.*, Collagen matrix deposition is dramatically enhanced in vitro when crowded with charged macromolecules: the biological relevance of the excluded volume effect, *FEBS Lett.*, 2007, **581**, 2709–2714, DOI: 10.1016/j.febslet.2007.05.020.

24 J. Y. Dewavrin, N. Hamzavi, V. P. Shim and M. Raghunath, Tuning the architecture of three-dimensional collagen hydrogels by physiological macromolecular crowding, *Acta Biomater.*, 2014, **10**, 4351–4359, DOI: 10.1016/j.actbio.2014.06.006.

25 V. Magno, *et al.*, Macromolecular crowding for tailoring tissue-derived fibrillated matrices, *Acta Biomater.*, 2017, **55**, 109–119, DOI: 10.1016/j.actbio.2017.04.018.

26 W. L. Ng, M. H. Goh, W. Y. Yeong and M. W. Naing, Applying macromolecular crowding to 3D bioprinting: fabrication of 3D hierarchical porous collagen-based hydrogel constructs, *Biomater. Sci.*, 2018, **6**, 562–574.

27 M. H. Lee, *et al.*, ECM microenvironment unlocks brown adipogenic potential of adult human bone marrow-derived MSCs, *Sci. Rep.*, 2016, **6**, 21173.

28 J. F. Bateman, W. G. Cole, J. J. Pillow and J. A. Ramshaw, Induction of procollagen processing in fibroblast cultures by neutral polymers, *J. Biol. Chem.*, 1986, **261**, 4198–4203.

29 J. Parkinson, K. E. Kadler and A. Brass, Simple physical model of collagen fibrillogenesis based on diffusion limited aggregation, *J. Mol. Biol.*, 1995, **247**, 823–831, DOI: 10.1006/jmbi.1994.0182.

30 T. J. Wess, in *Advances in Protein Chemistry*, Academic Press, 2005, vol. 70, pp. 341–374.

31 R. Rashid, *et al.*, Novel use for polyvinylpyrrolidone as a macromolecular crowder for enhanced extracellular matrix deposition and cell proliferation, *Tissue Eng., Part C*, 2014, **20**, 994–1002.

32 P. R. Salvalaggio, *et al.*, Islet filtration: a simple and rapid new purification procedure that avoids ficoll and improves islet mass and function, *Transplantation*, 2002, **74**, 877–879, DOI: 10.1097/01.tp.0000028781.41729.5b.

33 J. F. Bateman, W. G. Cole, J. J. Pillow and J. Ramshaw, Induction of procollagen processing in fibroblast cultures by neutral polymers, *J. Biol. Chem.*, 1986, **261**, 4198–4203.

34 G. Liu, *et al.*, Cytotoxicity study of polyethylene glycol derivatives, *RSC Adv.*, 2017, **7**, 18252–18259.

35 M. Lutolf and J. Hubbell, Synthetic biomaterials as instructive extracellular microenvironments for morphogenesis in tissue engineering, *Nat. Biotechnol.*, 2005, **23**, 47.

36 F. H. Silver and D. E. Birk, Kinetic analysis of collagen fibrillogenesis: I. Use of turbidity–time data, *Collagen Relat. Res.*, 1983, **3**, 393–405.

37 K. A. Rubinson and S. Krueger, Poly(ethylene glycol)s 2000-8000 in water may be planar: A small-angle neutron scattering (SANS) structure study, *Polymer*, 2009, **50**, 4852–4858.

38 I. M. Kuznetsova, K. K. Turoverov and V. N. Uversky, What macromolecular crowding can do to a protein, *Int. J. Mol. Sci.*, 2014, **15**, 23090–23140.

39 N. R. Lang, *et al.*, Estimating the 3D pore size distribution of biopolymer networks from directionally biased data, *Biophys. J.*, 2013, **105**, 1967–1975, DOI: 10.1016/j.bpj.2013.09.038.

40 K. Wolf, *et al.*, in *The Journal of cell biology*, 2013, vol. 201, pp. 1069–1084.

41 P. Banerjee, D. Lenz, J. P. Robinson, J. L. Rickus and A. K. Bhunia, A novel and simple cell-based detection system with a collagen-encapsulated B-lymphocyte cell line as a biosensor for rapid detection of pathogens and toxins, *Lab. Invest.*, 2008, **88**, 196–206, DOI: 10.1038/labinvest.3700703.

42 C. K. Choi, *et al.*, Actin and alpha-actinin orchestrate the assembly and maturation of nascent adhesions in a myosin II motor-independent manner, *Nat. Cell Biol.*, 2009, **10**, 1039–1050, DOI: 10.1038/ncb1763.

43 S. C. Wei, *et al.*, Matrix stiffness drives epithelial-mesenchymal transition and tumour metastasis through a TWIST1-G3BP2 mechanotransduction pathway, *Nat. Cell Biol.*, 2015, **17**, 678–688, DOI: 10.1038/ncb3157.

44 A. J. Engler, S. Sen, H. L. Sweeney and D. E. Discher, Matrix elasticity directs stem cell lineage specification, *Cell*, 2006, **126**, 677–689, DOI: 10.1016/j.cell.2006.06.044.

45 A. J. McKenzie, *et al.*, The mechanical microenvironment regulates ovarian cancer cell morphology, migration, and spheroid disaggregation, *Sci. Rep.*, 2018, **8**, 7228, DOI: 10.1038/s41598-018-25589-0.

 

46 N. Jain, K. V. Iyer, A. Kumar and G. V. Shivashankar, Cell geometric constraints induce modular gene-expression patterns via redistribution of HDAC3 regulated by actomyosin contractility, *Proc. Natl. Acad. Sci. U. S. A.*, 2013, **110**, 11349–11354, DOI: 10.1073/pnas.1300801110.

47 E. S. Sokol, *et al.*, Growth of human breast tissues from patient cells in 3D hydrogel scaffolds, *Breast Cancer Res.*, 2016, **18**, 19, DOI: 10.1186/s13058-016-0677-5.

48 B. Depalle, Z. Qin, S. J. Shefelbine and M. J. Buehler, Influence of cross-link structure, density and mechanical properties in the mesoscale deformation mechanisms of collagen fibrils, *J. Mech. Behav. Biomed. Mater.*, 2015, **52**, 1–13, DOI: 10.1016/j.jmbbm.2014.07.008.

49 J. Schnaub, T. Handler and J. A. Kas, Semiflexible Biopolymers in Bundled Arrangements, *Polymers*, 2016, **8**, 274, DOI: 10.3390/polym8080274.

50 S. M. Bezrukov, I. Vodyanoy and V. A. Parsegian, Counting polymers moving through a single ion channel, *Nature*, 1994, **370**, 279–281, DOI: 10.1038/370279a0.

51 V. A. Parsegian, R. P. Rand and D. C. Rau, Osmotic stress, crowding, preferential hydration, and binding: A comparison of perspectives, *Proc. Natl. Acad. Sci. U. S. A.*, 2000, **97**, 3987–3992.

52 A. Das, M. Monteiro, A. Barai, S. Kumar and S. Sen, MMP proteolytic activity regulates cancer invasiveness by modulating integrins, *Sci. Rep.*, 2017, **7**, 14219, DOI: 10.1038/s41598-017-14340-w.

53 S. Khetan, *et al.*, Degradation-mediated cellular traction directs stem cell fate in covalently crosslinked three-dimensional hydrogels, *Nat. Mater.*, 2013, **12**, 458–465, DOI: 10.1038/nmat3586.

54 N. J. Walters and E. Gentleman, Evolving insights in cell-matrix interactions: elucidating how non-soluble properties of the extracellular niche direct stem cell fate, *Acta Biomater.*, 2015, **11**, 3–16.

55 D. O. Velez, *et al.*, 3D collagen architecture induces a conserved migratory and transcriptional response linked to vasculogenic mimicry, *Nat. Commun.*, 2017, **8**, 1651.

56 V. M. Weaver, *et al.*, Reversion of the malignant phenotype of human breast cells in three-dimensional culture and in vivo by integrin blocking antibodies, *J. Cell Biol.*, 1997, **137**, 231–245.

57 S. A. Jimenez, R. I. Bashey, M. Benditt and R. Yankowski, Identification of collagen alpha1(I) trimer in embryonic chick tendons and calvaria, *Biochem. Biophys. Res. Commun.*, 1977, **78**, 1354–1361.

58 M. F. Coughlin and D. Stamenovic, A tensegrity model of the cytoskeleton in spread and round cells, *J. Biomech. Eng.*, 1999, **120**, 770–777.

59 D. E. Ingber, N. Wang and D. Stamenovic, Tensegrity, cellular biophysics, and the mechanics of living systems, *Rep. Prog. Phys.*, 2014, **77**, 046603, DOI: 10.1088/0034-4885/77/4/046603.

60 S. J. Evani, R. G. Prabhu, V. Gnanaruban, E. A. Finol and A. K. Ramasubramanian, Monocytes mediate metastatic breast tumor cell adhesion to endothelium under flow, *FASEB J.*, 2013, **27**, 3017–3029, DOI: 10.1096/fj.12-224824.

61 W. C. Huang, S. T. Chan, T. L. Yang, C. C. Tzeng and C. C. Chen, Inhibition of ICAM-1 gene expression, monocyte adhesion and cancer cell invasion by targeting IKK complex: molecular and functional study of novel alpha-methylene-gamma-butyrolactone derivatives, *Carcinogenesis*, 2004, **25**, 1925–1934, DOI: 10.1093/carcin/bgh211.

62 C. Schroder, *et al.*, Prognostic value of intercellular adhesion molecule (ICAM)-1 expression in breast cancer, *J. Cancer Res. Clin. Oncol.*, 2011, **137**, 1193–1201, DOI: 10.1007/s00432-011-0984-2.

63 G. S. Park and J. H. Kim, LPS Up-Regulates ICAM-1 Expression in Breast Cancer Cells by Stimulating a MyD88-BLT2-ERK-Linked Cascade, Which Promotes Adhesion to Monocytes, *Mol. Cells*, 2015, **38**, 821–828, DOI: 10.14348/molcells.2015.0174.

64 M. Aragona, *et al.*, A mechanical checkpoint controls multicellular growth through YAP/TAZ regulation by actin-processing factors, *Cell*, 2013, **154**, 1047–1059, DOI: 10.1016/j.cell.2013.07.042.

65 S. Dupont, *et al.*, Role of YAP/TAZ in mechanotransduction, *Nature*, 2011, **474**, 179–183, DOI: 10.1038/nature10137.

66 K. Wada, K. Itoga, T. Okano, S. Yonemura and H. Sasaki, Hippo pathway regulation by cell morphology and stress fibers, *Development*, 2011, **138**, 3907–3914, DOI: 10.1242/dev.070987.

67 G. Halder, S. Dupont and S. Piccolo, Transduction of mechanical and cytoskeletal cues by YAP and TAZ, *Nat. Rev. Mol. Cell Biol.*, 2012, **13**, 591–600, DOI: 10.1038/nrm3416.

68 M. Bao, J. Xie, A. Piruska and W. T. S. Huck, 3D microniches reveal the importance of cell size and shape, *Nat. Commun.*, 2017, **8**, 1962, DOI: 10.1038/s41467-017-02163-2.

69 Y. Kang and K. Pantel, Tumor cell dissemination: emerging biological insights from animal models and cancer patients, *Cancer Cell*, 2013, **23**, 573–581, DOI: 10.1016/j.ccr.2013.04.017.

70 C. Gaggioli, *et al.*, Fibroblast-led collective invasion of carcinoma cells with differing roles for RhoGTPases in leading and following cells, *Nat. Cell Biol.*, 2007, **9**, 1392–1400, DOI: 10.1038/ncb1658.

71 J. M. Hou, *et al.*, Clinical significance and molecular characteristics of circulating tumor cells and circulating tumor microemboli in patients with small-cell lung cancer, *J. Clin. Oncol.*, 2012, **30**, 525–532, DOI: 10.1200/jco.2010.33.3716.

72 S. Braun and B. Naume, Circulating and disseminated tumor cells, *J. Clin. Oncol.*, 2005, **23**, 1623–1626, DOI: 10.1200/jco.2005.10.073.

73 L. M. Jawerth, S. Münster, D. A. Vader, B. Fabry and D. A. Weitz, A Blind Spot in Confocal Reflection Microscopy: The Dependence of Fiber Brightness on Fiber Orientation in Imaging Biopolymer Networks, *Biophys. J.*, 2010, **98**, L1–L3, DOI: 10.1016/j.bpj.2009.09.065.

74 J. S. Bredfeldt, *et al.*, Computational segmentation of collagen fibers from second-harmonic generation images of breast cancer, *J. Biomed. Opt.*, 2014, **19**, 16007, DOI: 10.1117/1.jbo.19.1.016007.

75 D. Overby, J. Ruberti, H. Gong, T. F. Freddo and M. Johnson, Specific Hydraulic Conductivity of Corneal Stroma as Seen by Quick-Freeze/Deep-Etch, *J. Biomech. Eng.*, 2001, **123**, 154–161, DOI: 10.1115/1.1351888.

76 M. Haidekker, *Advanced Biomedical Image Analysis*, Wiley, 2011.

77 S. I. Fraley, *et al.*, Three-dimensional matrix fiber alignment modulates cell migration and MT1-MMP utility by spatially and temporally directing protrusions, *Sci. Rep.*, 2015, **5**, 14580, DOI: 10.1038/srep14580.

78 M. Radmacher, M. Fritz and P. K. Hansma, Imaging soft samples with the atomic force microscope: gelatin in water and propanol, *Biophys. J.*, 1995, **69**, 264–270, DOI: 10.1016/s0006-3495(95)79897-6.

79 A. J. Engler, F. Rehfeldt, S. Sen and D. E. Discher, Microtissue elasticity: measurements by atomic force microscopy and its influence on cell differentiation, *Methods Cell Biol.*, 2007, **83**, 521–545, DOI: 10.1016/s0091-679x(07)83022-6.

80 A. J. Engler, L. Richert, J. Y. Wong, C. Picart and D. E. Discher, Surface probe measurements of the elasticity of sectioned tissue, thin gels and polyelectrolyte multilayer films: Correlations between substrate stiffness and cell adhesion, *Surf. Sci.*, 2004, **570**, 142–154, DOI: 10.1016/j.susc.2004.06.179.

81 L. Richert, A. J. Engler, D. E. Discher and C. Picart, Elasticity of native and cross-linked polyelectrolyte multilayer films, *Biomacromolecules*, 2004, **5**, 1908–1916, DOI: 10.1021/bm0498023.

 